Z. Phys. C – Particles and Fields 47, 187–198 (1990)

Zeitschrift für Physik C Particles and Fields

Global jet properties at 14–44 GeV center of mass energy in e^+e^- annihilation

TASSO Collaboration

W. Braunschweig, R. Gerhards, F.J. Kirschfink[1], H.-U. Martyn
I. Physikalisches Institut der RWTH Aachen, Federal Republic of Germany[a]

H.M. Fischer, H. Hartmann, J. Hartmann, E. Hilger, A. Jocksch[2], R. Wedemeyer
Physikalisches Institut der Universität, Bonn, Federal Republic of Germany[a]

B. Foster, A.J. Martin[3]
H.H. Wills Physics Laboratory, University of Bristol, Bristol, UK[b]

E. Bernardi[4], J. Chwastowski[5], A. Eskreys[5], K. Genser[6], H. Hultschig, P. Joos, H. Kowalski, A. Ladage, B. Löhr, D. Lüke[7], P. Mättig[8], D. Notz, J.M. Pawlak[6], K.-U. Pösnecker, E. Ros, D. Trines, R. Walczak[6], G. Wolf
Deutsches Elektronen-Synchrotron DESY, Hamburg, Federal Republic of Germany

H. Kolanoski
Institut für Physik, Universität, Dortmund, Federal Republic of Germany[a]

J. Krüger, E. Lohrmann, G. Poelz, W. Zeuner[9]
II. Institut für Experimentalphysik der Universität, Hamburg, Federal Republic of Germany[a]

J. Hassard, J. Shulman[10], D. Su[11], I. Tomalin
Department of Physics, Imperial College, London, UK[b]

F. Barreiro, G. Cases, L. Hervas, J. del Peso
Universidad Autonoma de Madrid, Madrid, Spain[c]

M.G. Bowler, P.N. Burrows[12], R.J. Cashmore, M.E. Veitch
Department of Nuclear Physics, Oxford University, Oxford, UK[b]

J.C. Hart, D.H. Saxon
Rutherford Appleton Laboratory, Chilton, Didcot, UK[b]

S. Brandt, M. Holder
Fachbereich Physik der Universität-Gesamthochschule, Siegen, Federal Republic of Germany[a]

Y. Eisenberg, U. Karshon, A. Montag, D. Revel, E. Ronat[13], N. Wainer
Weizmann Institute, Rehovot, Israel[d]

A. Caldwell[14], D. Muller[15], S. Ritz[14], D. Strom[16], M. Takashima[9], Sau Lan Wu, G. Zobernig
Department of Physics, University of Wisconsin, Madison, WI, USA[e]

Received 13 February 1990

[1] Now at Lufthansa, Hamburg, FRG
[2] Now at Fa. Fichtner, Stuttgart, FRG
[3] Now at Queen Mary Westfield College, London
[4] Now at Robert Bosch GmbH, Schwieberdingen, FRG
[5] Now at Inst. of Nuclear Physics, Cracow, Poland
[6] Now at Warsaw University[f], Poland
[7] On leave at CERN, Geneva, Switzerland
[8] Now at IPP Canada, Carleton University, Ottawa, Canada
[9] Now at CERN, Geneva, Switzerland
[10] Now at University College, London
[11] Now at Rutherford Appleton Laboratory, Chilton, Didcot, UK
[12] Now at MIT, Cambridge, MA, USA
[13] deceased
[14] Now at Columbia University, NY USA
[15] Now at SLAC, California, CA, USA
[16] Now at University of Chicago, Chicago, IL, USA

[a] Supported by Bundesministerium für Forschung und Technologie
[b] Supported by UK Science and Engineering Research Council
[c] Supported by CAICYT
[d] Supported by the Minerva Gesellschaft für Forschung GmbH
[e] Supported by US Dept. of Energy, contract DE-AC02-76ER000881 and by US Nat. Sci. Foundation Grant number INT-8313994 for travel
[f] Partially supported by grant CPBP 01.06

Abstract. Jet properties in e^+e^- annihilation at center of mass energies of 14, 22, 35 and 43.7 GeV were studied with the data collected in the TASSO detector at PETRA, using the same evaluation procedures for all the energies. The total hadronic cross section ratio for the center of mass energy interval 39–47 GeV was determined to be $\mathcal{R}=4.11\pm0.05$ (stat.) ±0.18 (syst.) at $\langle\sqrt{s}\rangle=43.7$ GeV. Corrected distributions of global shape variables are presented as well as the inclusive charged particle distributions for scaled momentum and transverse momentum. The center of mass energy evolution of the average sphericity, thrust, aplanarity and particle momentum is shown.

1 Introduction

At present, properties of jets in e^+e^- annihilation can only be described by phenomenological models, characterized by a number of adjustable parameters. An additional handle to understand hadronization and to test the models is offered by the evolution of various jet properties with the center of mass energy. The PETRA storage ring has operated at center of mass energies between 12 and 47 GeV, offering a large range of energy for which such studies can be made. This paper complements an earlier study by our collaboration [1].

The data in this paper were analysed in terms of the total hadronic cross section, the event shape and the inclusive distributions, using the same numerical procedure at each center of mass energy, which resulted in a high degree of consistency of data sets at all four energies. This, together with the analysis of our 43.7 GeV data, implied reanalysis of the data at 14, 22 and 35 GeV.

2 Event and particle selection

The data were collected with the TASSO detector at the PETRA storage ring at DESY between 1979 and 1986 (see Table 1). The detector has been described elsewhere [2, 3]. The data acquisition and the event selection criteria were similar to those described in [4], but since they are important for the description of the systematic error estimation we repeat them briefly here:

Charged tracks were accepted if they satisfied the following requirements:

1) three-dimensional reconstruction;

Table 1. The data samples used in this analysis

Nominal energy	Range of c.m. energy (GeV)	Average c.m. energy (GeV)	$\int\mathcal{L}dt$ (pb^{-1})	No. of events
14 GeV	14.02–14.04	14.03	1.63	2704
22 GeV	21.98–22.00	21.99	2.79	1889
35 GeV	34.91–35.10	35.00	110	31175
44 GeV	39.32–46.78	43.70	35.0	6299

2) $|d_0|<5$ cm, where d_0 is the distance of the point of the closest approach to the origin in the plane perpendicular to the beam;

3) $p_{xy}>0.1$ GeV/c, where p_{xy} is the track momentum in the plane perpendicular to the beam;

4) $|\cos\Theta_{tr}|\leqq0.87$, where Θ_{tr} is the track polar angle;

5) $|z_0-z_v|<20$ cm, where z_0 is the track coordinate along the beam (which defines the z axis) at its closest approach to the origin and z_v is the z coordinate of the event vertex calculated with the tracks passing the above requirements.

A hadronic event was required to fulfill the following conditions:

1) at least 5 (4) good tracks for a center of mass energy $W>27$ GeV ($W\leqq27$ GeV);

2) the effective mass of the 3 particle system in events with 1 and 3 ($W\leqq15$ GeV) or 3 and 3 ($W\geqq15$ GeV) particles in each hemisphere (defined by the sphericity tensor) be greater than the τ mass;

3) for $W\leqq15$ GeV, at least one track in each hemisphere (defined with respect to the beam axis) and $|\sum Q|\leqq3$, where Q is the particle charge;

4) $|z_v|<6$ cm;

5) the momentum sum of accepted particles had to satisfy $\sum|p|>0.265\cdot W$.

The above conditions were imposed on the data during the offline analysis. At data taking there were trigger conditions equivalent to demanding a minimum number (2–5) of charged tracks with momentum larger than 0.25 GeV. In addition, independently, there were other conditions the most important one being a trigger on the energy seen in the calorimeters.

In order to suppress events with hard photon radiation in the initial state, and to ensure a large acceptance for the particles in the jets, additional cuts were made. It was required that $|\cos\Theta_n|>0.20$, where Θ_n is the angle between the normal to the event plane and the beam direction and $|\cos\Theta_S|\leqq0.7$, where Θ_S is the angle between the sphericity tensor axis and the beam direction. To avoid distortions in the event shape variable distributions, all particle momenta which were reconstructed to be larger than 1.5 times beam momentum, were rescaled (conserving the direction) to be equal to $1.5\cdot p_{beam}$.

3 Monte Carlo event generator

To correct the data a Monte Carlo program [5, 6] was used. Two options for calculating the initial parton configuration were employed, namely the Lund cascade [7] option (Lund LLA$+O(\alpha_s)$) and a matrix element [8] option (Lund $O(\alpha_s^2)$) (α_s denotes the strong coupling constant). Since the event generator is used to calculate the corrections for the data, some of its parameters were adjusted to get an agreement between the data and the Monte Carlo. A tuning method similar to that of previous TASSO publications [1, 9] was applied. Several distributions were used to tune the parameters, namely

$(1/N)\,dN/dQ_2$, $(1/N)\,dN/dQ_1$, $(1/N)\,dN/dL_2$, $(1/N)\,dN/dL_1$, $(1/\sigma_{tot})\,d\sigma/dp_{\perp in}^{(S)}$, $(1/\sigma_{tot})\,d\sigma/dp_{\perp out}^{(S)}$, $(1/\sigma_{tot})\,d\sigma/dp_{\perp in}^{(P)}$, $(1/\sigma_{tot})\,d\sigma/dp_{\perp out}^{(P)}$, and $(1/\sigma_{tot})\,d\sigma/dx$. Here Q_1, Q_2 and L_1, L_2 are the smallest and next to the smallest eigenvalues of the sphericity [10] and the first order momentum [11] tensors respectively; $p_{\perp in}$, $p_{\perp out}$ are the transverse momentum components in and out of the event plane defined by the plane perpendicular to the eigenvector corresponding to the smallest eigenvalues of the tensors. The S or P superscripts denote $p_\perp$ calculated with respect to the sphericity tensor axis or the first order momentum tensor axis respectively, and x is defined by $2p/W$, where W is the center of mass energy. One should stress that the Monte Carlo was used here as a tool to obtain the corrected data and not with a view to determine physical parameters.

The tuned parameters, obtained in a simultaneous fit, were: the QCD scale parameter Λ, σ_q related to the r.m.s. of the Gaussian $p_\perp$ quark spectrum $e^{-p_\perp^2/2\sigma_q^2}$ and the parameters a and b of the Lund fragmentation function [12]

$$f(z)=\frac{1}{z}(1-z)^a e^{-\frac{bm_\perp^2}{z}}; \quad m_\perp^2=p_\perp^2+m^2,$$

where z is the fraction of remaining $E+p_\parallel$ (energy plus longitudinal momentum) taken by a hadron. This function was used for the light quarks only. For b and c quarks the Peterson fragmentation function [13]

$$f(z)\sim\frac{1}{z\left(1-\frac{1}{z}-\frac{\varepsilon_q}{1-z}\right)^2}$$

was used. Different sets of Peterson fragmentation parameters, close to those determined previously by TASSO [14, 15], were tried while performing the fits described below and $\varepsilon_c=0.07$, $\varepsilon_b=0.01$ gave the best description of the data and were used in the further analysis. In fits with the Lund fragmentation function used for all quark flavours the χ^2 of the fit was about 20% higher than with the Peterson fragmentation function.

To save computer time the tuning was performed to corrected data described below and an iterative procedure was applied until agreement between the data and fully simulated Monte Carlo events, expressed in terms of χ^2, was acceptable or it was not possible to obtain a further significant decrease of χ^2. In the case of Lund LLA$+O(\alpha_s)$ the fit was performed at 43.7 GeV only and the Monte Carlo with those parameters properly described the data at lower energies. In the case of Lund $O(\alpha_s^2)$ it was found necessary to perform a separate fit also at 35 GeV.

Table 2 shows final parameter values of the Lund $O(\alpha_s^2)$ and Lund LLA$+O(\alpha_s)$ programs used at each center of mass energy. The number of Monte Carlo events produced with the full detector simulation are also shown.

Table 3 shows χ^2 for some uncorrected ("raw") distributions, compared with the fully simulated Monte Carlo events, including radiative corrections, background contamination, detector response, event reconstruction and selection cuts. Since at each energy the number of events in the Monte Carlo sample was significantly bigger than the number of the data events, the χ^2 are dominated by the statistical errors on the data. While making comparisons of χ^2 for two different energies one should remember that the number of events in the data is different at different center of mass energies and that χ^2, by its nature, increases with the number of events. The number of Monte Carlo events was the same for each option. From the table one can see that the overall agreement between the data and the Lund LLA$+O(\alpha_s)$ Monte Carlo at 43.7 GeV is sufficiently good for our purpose, as mentioned above. As mentioned already the Lund LLA$+O(\alpha_s)$ Monte Carlo was run with the same parameters at all energies and the agreement between the data and the Monte Carlo was rather good. The agreement for the Lund $O(\alpha_s^2)$ Monte Carlo is still satisfactory, although two sets of parameters had to be used.

Table 2. Number of events produced and parameter values of Lund $O(\alpha_s^2)$ and Lund LLA$+O(\alpha_s^2)$ programs used while correcting the data at $\bar{W}=14$, 22, 35 and 44 GeV

	14 GeV	22 GeV	35 GeV	44 GeV
Lund LLA$+O(\alpha_s)$				
Λ_{LLA} [GeV]		0.44		
a		0.87		
b [c^4/GeV^2]		1.05		
σ_q [GeV/c]		0.37		
Lund $O(\alpha_s^2)$				
$\Lambda_{\overline{MS}}$ [GeV]		0.57		0.74
a		0.96		1.10
b [c^4/GeV^2]		0.70[a]		0.84
σ_q [GeV/c]		0.40		0.42
No. of MC events	12740	8450	75120	30560
No. of data events	2704	1889	31175	6299

[a] fixed at the default value

Table 3. χ^2 per degree of freedom for some uncorrected distributions at $\bar{W}=14$, 22, 35 and 44 GeV as a measure of the agreement between the data and the Monte Carlo simulation. LM and LL denote Lund $O(\alpha_s^2)$ and Lund LLA$+O(\alpha_s)$ Monte Carlo

Variable	14 GeV		22 GeV		35 GeV		44 GeV	
	LM	LL	LM	LL	LM	LL	LM	LL
n_{ch}	2.1	0.75	1.6	0.37	5.2	2.4	1.4	0.99
x_p	2.2	2.3	1.2	1.2	5.8	5.5	2.2	1.5
S	1.8	1.3	0.95	0.57	1.0	1.4	1.9	0.68
A	1.3	1.4	0.64	0.99	8.0	1.3	3.7	1.1
T	3.0	1.4	0.89	0.33	2.4	1.7	3.2	2.3

4 The total cross section

The total cross section for annihilation into hadrons according to the reaction $e^+e^-\to$ hadrons was determined

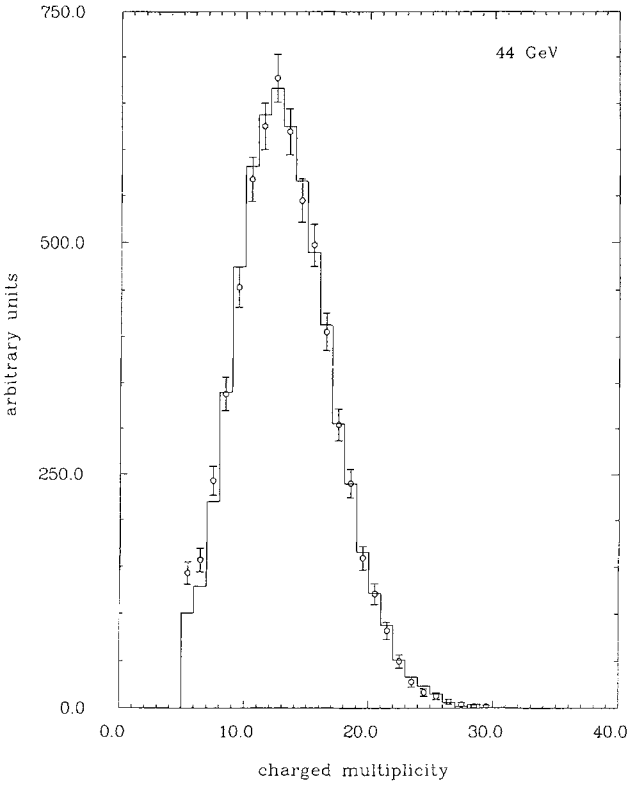

Fig. 1. Uncorrected charged multiplicity distribution at $\bar{W}=44$ GeV. The points represent the data, the full line shows the Monte Carlo prediction

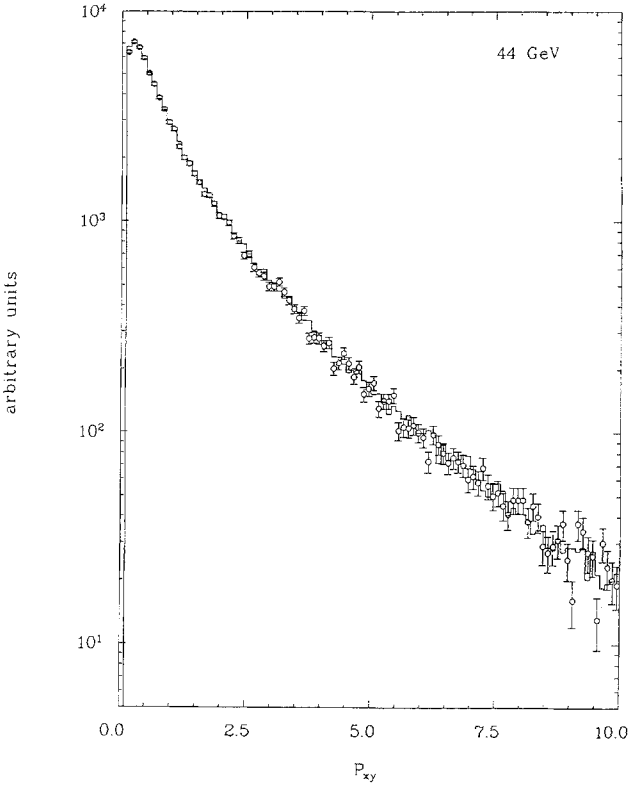

Fig. 3. Uncorrected p_{xy} distribution at $\bar{W}=44$ GeV. The points represent the data, the full line shows the Monte Carlo prediction

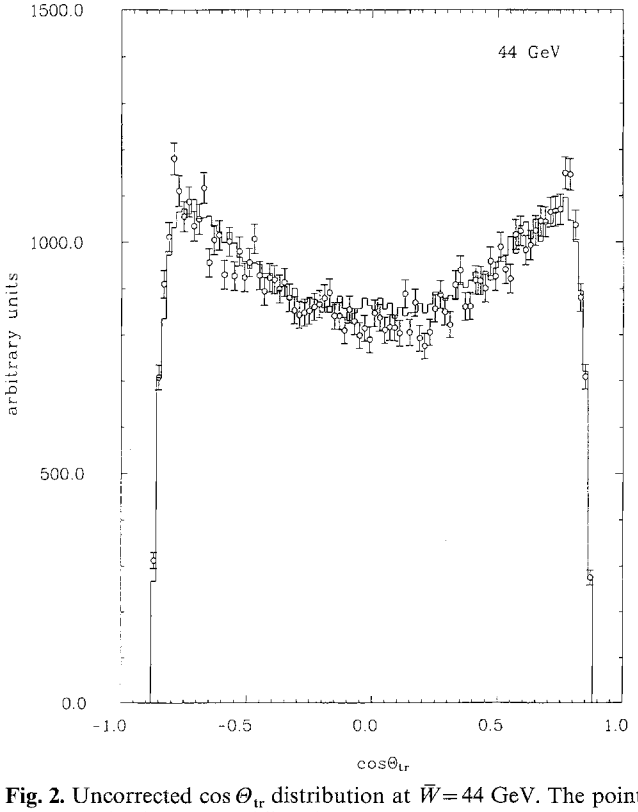

Fig. 2. Uncorrected $\cos\Theta_{tr}$ distribution at $\bar{W}=44$ GeV. The points represent the data, the full line shows the Monte Carlo prediction

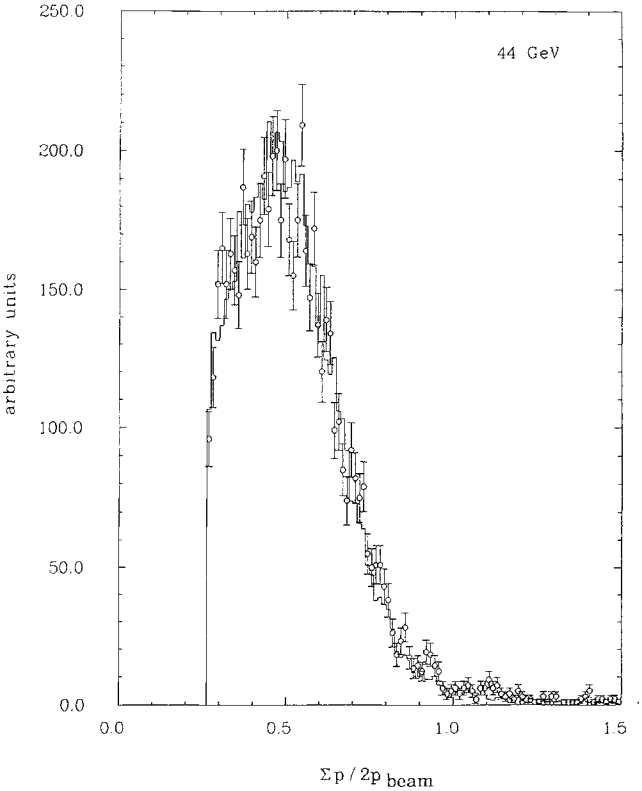

Fig. 4. Uncorrected $\sum|p|/2p_{\text{beam}}$ distribution at $\bar{W}=44$ GeV. The points represent the data, the full line shows the Monte Carlo prediction

by evaluating the acceptance ε for Monte Carlo events with QED radiative corrections [16] applied. The final result was obtained from the equation:

$$\sigma_{\text{tot}} = \frac{N_{\text{meas}}}{\mathscr{L}\varepsilon(1+\delta)}$$

where $\mathscr{L}$ is the collected luminosity and δ is the correction for the increase of the cross section due to the QED radiative effects. The hadronic cross section was then expressed by its ratio $\mathscr{R}$ to the theoretical cross section σ_0 for the process $e^+e^- \to \mu^+\mu^-$ calculated in the lowest order of QED.

To make sure that the acceptance was calculated properly, distributions of the variables used to make the selection cuts were studied. Figures 1–4 show a comparison of uncorrected distributions of charged multiplicity n_{ch}, track polar angle $\cos\Theta_{\text{tr}}$, particle momentum perpendicular to the beam p_{xy} and $\sum|p|/W$ as measured with the TASSO detector at a center of mass energy of 43.7 GeV with the fully simulated Lund LLA $+ O(\alpha_s)$ Monte Carlo events, including radiative QED corrections, background, detector response, event reconstruction and selection cuts. Despite some small discrepancies the overall agreement between the data and the Monte Carlo is good. The measured value of $\mathscr{R}$ at 43.7 GeV is $\mathscr{R} = 4.113 \pm 0.052$ (stat.) ± 0.085 (syst.). The systematic error was estimated by varying the selection criteria, including the trigger condition, and by changing the option of the generator from Lund LLA $+ O(\alpha_s)$ to Lund $O(\alpha_s^2)$. The contributions to the systematic error coming from the changes in the various cuts and conditions are summarized in Table 4.

We are adding an additional systematic error of 3.0% coming from the luminosity measurement and 2.5% [17, 18] coming from uncertainties in the radiative corrections and for higher order effects, which have been neglected. The final result including all the errors reads:

$$\mathscr{R} = 4.11 \pm 0.05 \text{ (stat.)} \pm 0.18 \text{ (syst.)}.$$

and is in a good agreement with the results of other PETRA experiments [19, 20, 21]. The $\mathscr{R}$ values calculated in this analysis for 14, 22, 35, and 43.7 GeV are presented in Table 5. The values at 14 and 22 GeV are very close to our old results [4, 17]. The value at 35 GeV is based on new data as compared to [4, 17]; it agrees with results published there. The 43.7 GeV data include all the statistics from [18]; also at this energy the new cross section value agrees with the old ones.

Table 4. Cuts and conditions used for systematic error estimation at 14, 22, 35 and 44 GeV and contributions to the systematic error of $\mathscr{R}$ at $\bar{W} = 44$ GeV

Condition varied	Standard condition	Contribution to the systematic error of $\mathscr{R}$
$\lvert d_0\rvert \leqq 3$ cm	$\leqq 5$ cm	0.45%
$p_{xy} \geqq 0.2$ GeV	$\geqq 0.1$ GeV	0.21%
$\lvert\cos\Theta_{\text{tr}}\rvert \leqq 0.8$	$\leqq 0.87$	0.63%
$\lvert z_{\text{tr}} - z_{\text{vert}}\rvert \leqq 15$ cm	$\leqq 20$ cm	0.51%
$n_{\text{ch}} \geqq 7\,(6)$	$\geqq 5\,(4)$	1.16%
$\lvert\cos\Theta_S\rvert \leqq 0.65$	$\leqq 0.70$	–
$\frac{\sum p}{W} \geqq 0.3$	$\geqq 0.265$	0.11%
only events with the track trigger on	all events	1.16%
Lund $O(\alpha_s^2)$ MC used	Lund LLA $+ O(\alpha_s)$	0.07%

Table 5. Total hadronic cross section ratio $\mathscr{R}$ for $\bar{W} = 14$, 22, 35 and 44 GeV

$\bar{W}$	$\mathscr{R}$
14.03	$4.12 \pm 0.08 \pm 0.11 \pm 0.16$[a] 4.12 ± 0.21
21.99	$3.86 \pm 0.09 \pm 0.08 \pm 0.15$ 3.86 ± 0.19
35.00	$4.15 \pm 0.02 \pm 0.08 \pm 0.16$ 4.15 ± 0.18
43.70	$4.11 \pm 0.05 \pm 0.08 \pm 0.16$ 4.11 ± 0.19

[a] The first error is statistical, the second is systematic coming from selection cuts and Monte Carlo, the third is systematic coming from luminosity measurement and missing terms in the radiative corrections calculations. The value in the second row presents all the errors combined in quadrature

5 Inclusive particle momentum and event variable distributions

5.1 Corrections

The distributions presented in this section were obtained by correcting the measured distributions for initial state radiation, background contamination from $\tau^+\tau^-$ and $\gamma\gamma$ processes [22], particle decays, detector effects and selection procedure.

The correction procedure was similar to that in [4]: first, a set of N_{gen} events was generated using a Monte Carlo program at a fixed center of mass energy with no QED radiative corrections, yielding the distributions $n_{\text{gen}}(x)$ of charged particles for different intervals of an observable x. All the primary produced particles or those produced in the decay of particles with an average lifetime smaller than $3 \cdot 10^{-10}$ s were considered. For this event sample the sphericity and thrust axes distributions were derived not only from the charged particles, as in the case of all the other distributions, but from both charged and neutral particles.

Secondly, both hadronic and background events were generated including QED radiative effects and were followed through the TASSO detector simulation program, generating hits in the tracking chambers. Energy loss, multiple scattering, photon conversions, nuclear interactions in the material of the detector and particle decays as well as the detector efficiency, resolution, noise and cross-talk were taken into account. The events were then passed through the same track finding and reconstruction programs and through the reduction programs

as used for the real data, yielding N_{det} accepted events, corresponding to the distributions $n_{\text{det}}(x)$. For every bin i of every distribution $n(x)$, a correction factor $C^i(x)$ was calculated

$$C^i(x)=\frac{n^i_{\text{gen}}(x)}{N_{\text{gen}}}\Big/\frac{n^i_{\text{det}}(x)}{N_{\text{det}}}.$$

The corrected distributions $n^i_{\text{corr}}(x)$ were then derived from the measured distributions $n^i_{\text{meas}}(x)$ for a total of N_{meas} events, using the formula

$$n^i_{\text{corr}}(x)=C^i(x)\frac{n^i_{\text{meas}}(x)}{N_{\text{meas}}}.$$

The above definition implies that the distributions $n^i_{\text{corr}}(x)$ are normalized to one event for global event variables and to the average accepted charged multiplicity for inclusive distributions.

5.2 *Statistical and systematic errors*

The statistical errors are dominated by those of the data. At all center of mass energies two types of systematic error were considered, namely those coming from the differences between the data and the Monte Carlo and those coming from the type of Monte Carlo used. The former were estimated by changing the selection cuts and trigger condition, the latter by taking the difference between the corrected distributions obtained with the Lund LLA+$O(\alpha_s)$ and Lund $O(\alpha_s^2)$ Monte Carlo.

Table 4 itemizes the systematic error sources influencing the distributions of the studied quantities. For each bin of each distribution and for the average values, the errors shown below are the sums in quadrature of statistical and systematic errors.

5.3 *Inclusive momentum distributions*

Figure 5 and Table 6 present the normalized cross section $(1/\sigma_{\text{tot}})\,d\sigma/dx$, where x is the fractional particle momentum, $x=2p/W$. The data presented in Table 6 show some disagreement as compared with the old TASSO

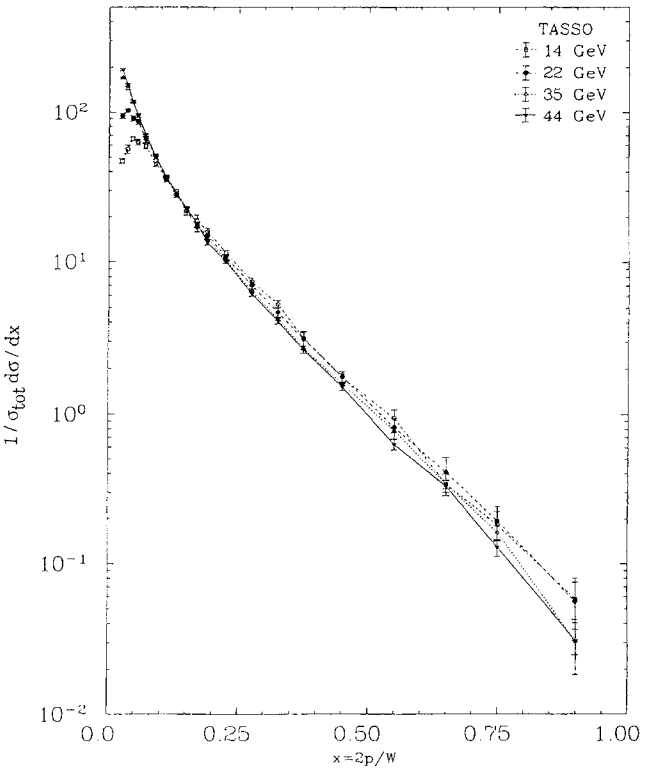

Fig. 5. Normalized scaled momentum distributions $(1/\sigma_{\text{tot}})\,d\sigma/dx$, where $x=2p/W$ at $\bar{W}=14$, 22, 35 and 44 GeV. The lines join the corresponding points for clarity

Table 6. Normalized scaled momentum distributions $(1/\sigma_{\text{tot}})\,d\sigma/dx$, where $x=2p/W$. In the calculation of $\langle x\rangle$ the interval $0<x<0.02$ was included

x	14 GeV	22 GeV	35 GeV	44 GeV
0.02–0.03	47.2 ±1.7	94.0 ±3.9	169.3 ±2.4	191.8 ±3.9
0.03–0.04	56.5 ±3.6	102.2 ±3.3	143.7 ±2.7	152.7 ±3.0
0.04–0.05	66.3 ±2.1	90.7 ±3.9	115.5 ±1.6	118.5 ±2.9
0.05–0.06	62.9 ±2.7	85.9 ±3.6	93.3 ±1.5	95.0 ±2.7
0.06–0.08	58.0 ±2.3	65.7 ±2.0	69.2 ±1.2	70.5 ±1.3
0.08–0.10	44.9 ±1.7	50.3 ±2.1	49.7 ±1.1	49.0 ±1.7
0.10–0.12	36.1 ±1.3	35.4 ±1.5	36.33 ±0.43	37.17 ±0.89
0.12–0.14	29.4 ±1.0	27.0 ±1.3	28.08 ±0.37	28.67 ±0.84
0.14–0.16	22.05 ±0.96	21.8 ±1.3	22.43 ±0.35	22.66 ±0.61
0.16–0.18	18.9 ±1.7	17.1 ±1.2	18.02 ±0.31	17.79 ±0.76
0.18–0.20	16.01 ±0.95	15.16 ±0.95	14.38 ±0.28	13.45 ±0.47
0.20–0.25	11.58 ±0.42	10.78 ±0.47	10.24 ±0.16	10.06 ±0.32
0.25–0.30	7.44 ±0.48	7.05 ±0.38	6.43 ±0.11	6.18 ±0.23
0.30–0.35	5.28 ±0.30	4.65 ±0.38	4.23 ±0.10	4.08 ±0.18
0.35–0.40	3.15 ±0.35	3.13 ±0.32	2.719 ±0.087	2.66 ±0.14
0.40–0.50	1.75 ±0.11	1.76 ±0.15	1.587 ±0.037	1.517 ±0.072
0.50–0.60	0.95 ±0.13	0.82 ±0.13	0.782 ±0.028	0.631 ±0.052
0.60–0.70	0.342 ±0.056	0.41 ±0.11	0.341 ±0.023	0.331 ±0.031
0.70–0.80	0.181 ±0.041	0.193 ±0.050	0.162 ±0.018	0.129 ±0.017
0.80–1.00	0.058 ±0.017	0.056 ±0.025	0.030 ±0.012	0.0309±0.0059
$\langle x\rangle$	0.1302±0.0023	0.1102±0.0020	0.0908±0.0008	0.0839±0.0009

Table 7. Normalized scaled momentum distributions $(1/\sigma_{tot})\, d\sigma/dx$, shown in the binning used in fits

x	14 GeV	22 GeV	35 GeV	44 GeV
0.02–0.05	56.4 ±3.9	95.4 ±2.6	142.9 ±2.0	154.4 ±2.4
0.05–0.10	54.1 ±1.7	63.6 ±1.6	66.23 ±0.92	67.2 ±1.2
0.10–0.20	24.51 ±0.46	23.48±0.49	23.85 ±0.18	23.95 ±0.38
0.20–0.30	9.51 ±0.28	8.92±0.29	8.335±0.098	8.12 ±0.20
0.30–0.40	4.21 ±0.22	3.89±0.19	3.476±0.069	3.37 ±0.12
0.40–0.50	1.75 ±0.11	1.76±0.15	1.587±0.037	1.517±0.072
0.50–0.70	0.640±0.061	0.61±0.10	0.562±0.019	0.484±0.031

results [4] at 14–35 GeV center of mass energy. Since data presented here were corrected with more realistic Monte Carlo methods, they are more reliable and supersede our earlier results.

The energy dependence of the differential cross section is better seen in Fig. 6 and Table 7, which show $(1/\sigma_{tot})\, d\sigma/dx$ for fixed x intervals plotted versus $s = W^2$. The amount of the scale breaking can be quantified by fitting the data to the following form suggested by QCD [23, 34]

$$1/\sigma_{tot}\, d\sigma/dx = c_1(1 + c_2 \ln(s/s_0))$$

with

$$s_0 = 1 \text{ GeV}^2.$$

The result of the fit is given in Table 8. Note that $\partial((1/\sigma_{tot})\, d\sigma/dx)/\partial \ln s = c_1 c_2$ and that the quoted errors have been calculated taking full account of correlations between c_1 and c_2. There are significant scaling violations. In Fig. 6 the results of the Lund LLA + $O(\alpha_s)$ and Lund $O(\alpha_s^2)$ Monte Carlo are shown also. The Monte Carlo parameters are those given in Table 2. One can see that the Lund programs represent the data and its energy dependence quite well.

Table 8. Fit results to the s-dependence of the scaled cross section $(1/\sigma_{tot})\, d\sigma/dx = c_1(1 + c_2 \ln(s/s_0))$, where $s_0 = 1$ GeV^2

x	c_1	c_2	$c_1 \cdot c_2$
0.02–0.05	−179 ±12	−0.2498±0.0070	44.6 ±1.7
0.05–0.10	28.0 ± 6.8	0.191 ±0.068	5.33 ±0.82
0.10–0.20	25.2 ± 1.6	−0.0072±0.0087	−0.18 ±0.23
0.20–0.30	12.75± 0.95	−0.0486±0.0071	−0.62 ±0.14
0.30–0.40	6.22± 0.70	−0.0615±0.0090	−0.383±0.099
0.40–0.50	2.34± 0.37	−0.045 ±0.015	−0.107±0.053
0.50–0.70	1.03± 0.21	−0.066 ±0.015	−0.068±0.029

Another way of looking at the scaled momentum distribution (usually employed in multigluon emission studies, see e.g. [25] and references therein) is to plot $x\, d\sigma/dx$ versus $\ln(1/x)$ instead of plotting $d\sigma/dx$ against x, which allows one to have a closer look at the low x values. From Fig. 7 (Table 9) one can clearly see that

Table 9. Normalized $\ln(1/x)$ distributions $(1/\sigma_{tot})\, d\sigma/d\ln(1/x)$, where $x = 2p/W$

$\ln(1/x)$	14 GeV	22 GeV	35 GeV	44 GeV
0.0–0.2	0.052±0.026	0.033±0.016	0.0222±0.0088	0.0195±0.0043
0.2–0.4	0.140±0.025	0.164±0.056	0.127 ±0.013	0.111 ±0.015
0.4–0.6	0.325±0.047	0.351±0.086	0.297 ±0.013	0.257 ±0.022
0.6–0.8	0.624±0.068	0.581±0.067	0.559 ±0.020	0.474 ±0.057
0.8–1.0	0.95 ±0.10	0.986±0.084	0.860 ±0.026	0.865 ±0.046
1.0–1.2	1.620±0.085	1.46 ±0.13	1.256 ±0.028	1.277 ±0.053
1.2–1.4	2.02 ±0.11	1.88 ±0.13	1.780 ±0.033	1.663 ±0.070
1.4–1.6	2.68 ±0.11	2.45 ±0.16	2.294 ±0.042	2.259 ±0.078
1.6–1.8	3.09 ±0.12	2.86 ±0.14	2.888 ±0.040	2.798 ±0.094
1.8–2.0	3.49 ±0.15	3.31 ±0.15	3.369 ±0.047	3.367 ±0.098
2.0–2.2	3.81 ±0.13	3.67 ±0.16	3.741 ±0.042	3.855 ±0.098
2.2–2.4	3.99 ±0.16	4.26 ±0.19	4.264 ±0.078	4.26 ±0.13
2.4–2.6	4.08 ±0.15	4.68 ±0.19	4.587 ±0.076	4.66 ±0.18
2.6–2.8	3.98 ±0.30	4.63 ±0.27	4.878 ±0.067	4.99 ±0.11
2.8–3.0	3.44 ±0.16	4.74 ±0.26	5.106 ±0.083	5.23 ±0.12
3.0–3.2	2.97 ±0.14	4.03 ±0.19	5.244 ±0.080	5.31 ±0.13
3.2–3.4	2.19 ±0.15	3.71 ±0.14	5.100 ±0.070	5.40 ±0.16
3.4–3.6	1.63 ±0.13	3.13 ±0.16	4.737 ±0.080	5.25 ±0.12
3.6–3.8	1.198±0.070	2.31 ±0.15	4.206 ±0.081	4.68 ±0.10
3.8–4.0	0.799±0.061	1.72 ±0.19	3.532 ±0.086	4.26 ±0.10
4.0–4.2	0.478±0.095	1.257±0.083	2.734 ±0.068	3.41 ±0.10
4.2–4.4		0.953±0.073	2.082 ±0.064	2.784 ±0.075
4.4–4.6		0.56 ±0.10	1.487 ±0.075	2.08 ±0.10
4.6–4.8			1.051 ±0.022	1.566 ±0.072
4.8–5.0			0.632 ±0.044	1.053 ±0.049

Table 10. Normalized transverse momentum distributions $(1/\sigma_{tot})\, d\sigma/dp_\perp$ GeV/c)$^{-1}$

$p_\perp$ (GeV/c)	14 GeV	22 GeV	35 GeV	44 GeV
0.00–0.05	6.11 ±0.49	6.79 ±0.46	7.70 ±0.38	8.50 ±0.49
0.05–0.10	12.11 ±0.73	14.29 ±0.66	16.43 ±0.45	17.70 ±0.92
0.10–0.15	17.03 ±0.96	18.1 ±1.0	21.96 ±0.41	23.19 ±0.62
0.15–0.20	18.65 ±0.81	21.5 ±1.1	24.96 ±0.46	25.54 ±0.64
0.20–0.25	18.28 ±0.90	21.58 ±0.87	25.43 ±0.45	26.08 ±0.67
0.25–0.30	19.10 ±0.65	21.3 ±1.5	23.95 ±0.36	24.00 ±0.56
0.30–0.35	16.31 ±0.83	18.97 ±0.75	21.88 ±0.29	22.69 ±0.60
0.35–0.40	14.19 ±0.90	16.7 ±1.0	19.13 ±0.56	19.48 ±0.58
0.40–0.45	11.30 ±0.85	13.71 ±0.74	16.50 ±0.24	17.94 ±0.59
0.45–0.50	9.33 ±0.48	12.03 ±0.76	14.35 ±0.22	15.02 ±0.45
0.50–0.60	6.73 ±0.33	8.47 ±0.44	11.04 ±0.16	12.17 ±0.28
0.60–0.70	4.46 ±0.29	6.02 ±0.42	7.73 ±0.14	8.69 ±0.22
0.70–0.80	2.48 ±0.19	4.15 ±0.25	5.49 ±0.10	6.27 ±0.23
0.80–0.90	1.69 ±0.19	2.52 ±0.29	4.008 ±0.085	4.43 ±0.25
0.90–1.00	0.89 ±0.10	1.84 ±0.19	2.810 ±0.077	3.30 ±0.16
1.00–1.20	0.589 ±0.088	1.03 ±0.12	1.786 ±0.054	2.344 ±0.077
1.20–1.40	0.196 ±0.040	0.51 ±0.11	1.049 ±0.039	1.338 ±0.057
1.40–1.60	0.082 ±0.041	0.269 ±0.058	0.622 ±0.038	0.846 ±0.044
1.60–1.80	0.030 ±0.018	0.164 ±0.046	0.379 ±0.019	0.563 ±0.036
1.80–2.00	0.030 ±0.022	0.123 ±0.053	0.239 ±0.016	0.412 ±0.034
2.00–2.50		0.070 ±0.035	0.1261 ±0.0066	0.229 ±0.016
2.50–3.00		0.0086 ±0.0059	0.0500 ±0.0048	0.087 ±0.016
3.00–4.00			0.0155 ±0.0018	0.0385 ±0.0050
4.00–6.00			0.00320 ±0.00071	0.0068 ±0.0016
$\langle p_\perp \rangle$	0.3466 ±0.0056	0.3889 ±0.0064	0.4342 ±0.0038	0.4695 ±0.0049

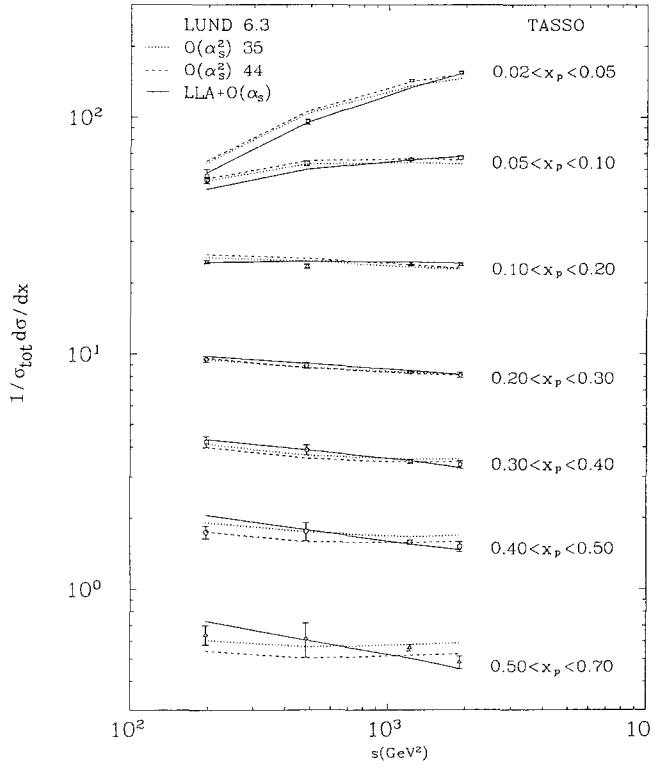

Fig. 6. Normalized scaled momentum distributions $(1/\sigma_{tot})\, d\sigma/dx$ versus $s = W^2$ for different x intervals. The lines show predictions of Lund LLA + $O(\alpha_s)$ and Lund $O(\alpha_s^2)$ Monte Carlo with the parameters as described in Sect. 3 and Table 2

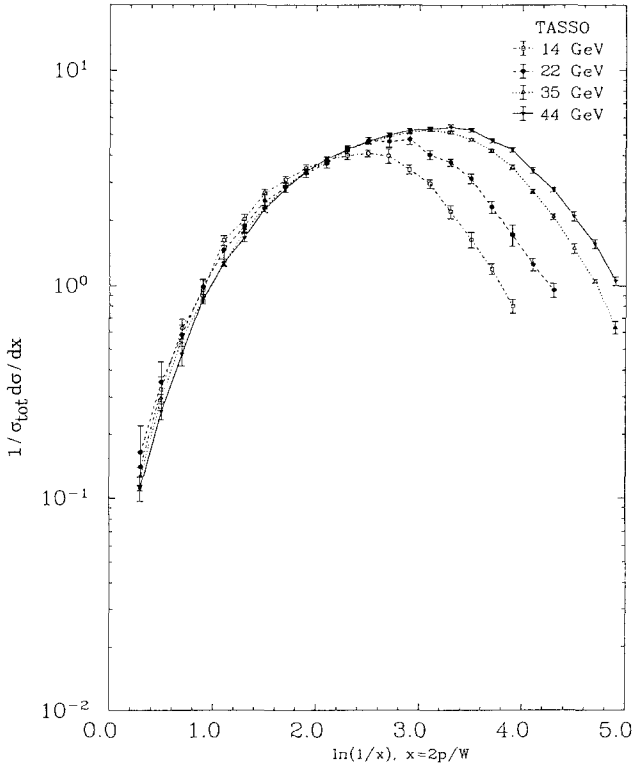

Fig. 7. Normalized $\ln(1/x)$ distributions $(1/\sigma_{tot})\, d\sigma/d\ln(1/x)$, where $x = 2p/W$ at $\bar{W} = 14$, 22, 35 and 44 GeV. The lines join the corresponding points for clarity

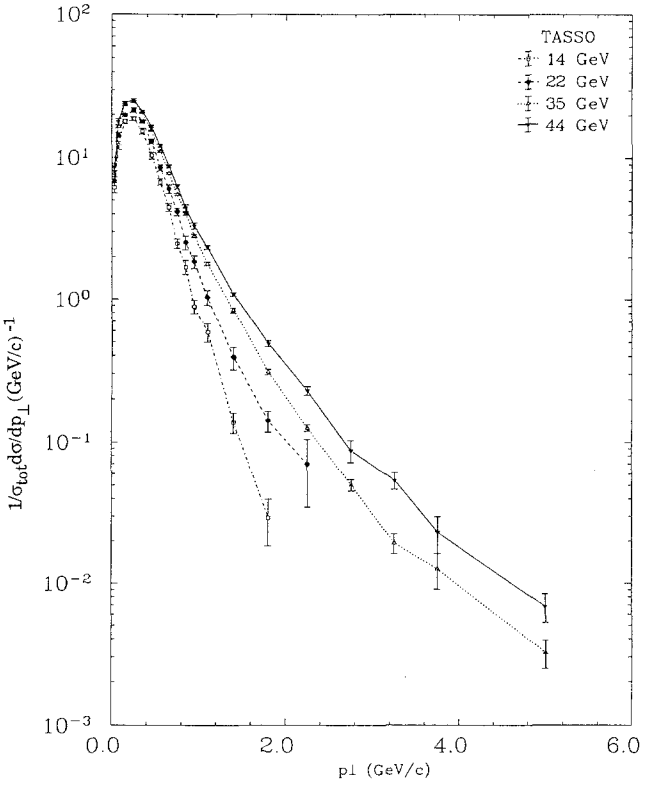

Fig. 8. Normalized transverse momentum distributions $(1/\sigma_{tot})\, d\sigma/dp_\perp$ (GeV/c)$^{-1}$ at $\bar{W}=14$, 22, 35 and 44 GeV. The lines join the corresponding points for clarity

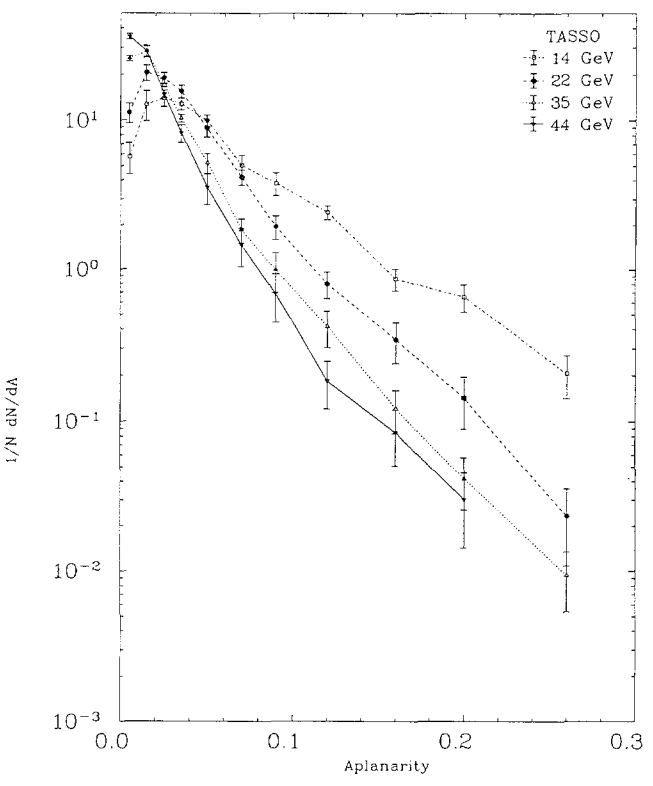

Fig. 10. Normalized aplanarity distributions $(1/N)\, dN/dA$ at $\bar{W}=14$, 22, 35 and 44 GeV. The lines join the corresponding points for clarity

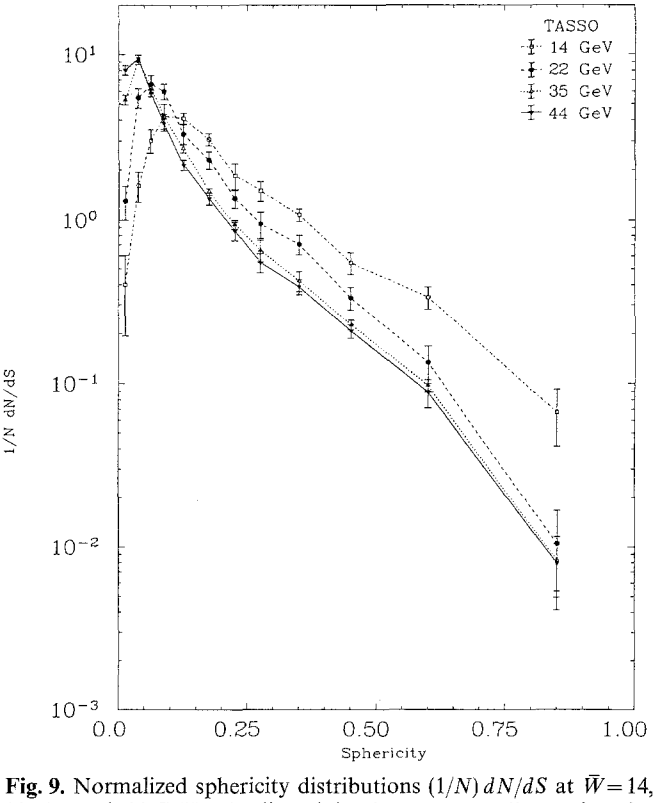

Fig. 9. Normalized sphericity distributions $(1/N)\, dN/dS$ at $\bar{W}=14$, 22, 35 and 44 GeV. The lines join the corresponding points for clarity

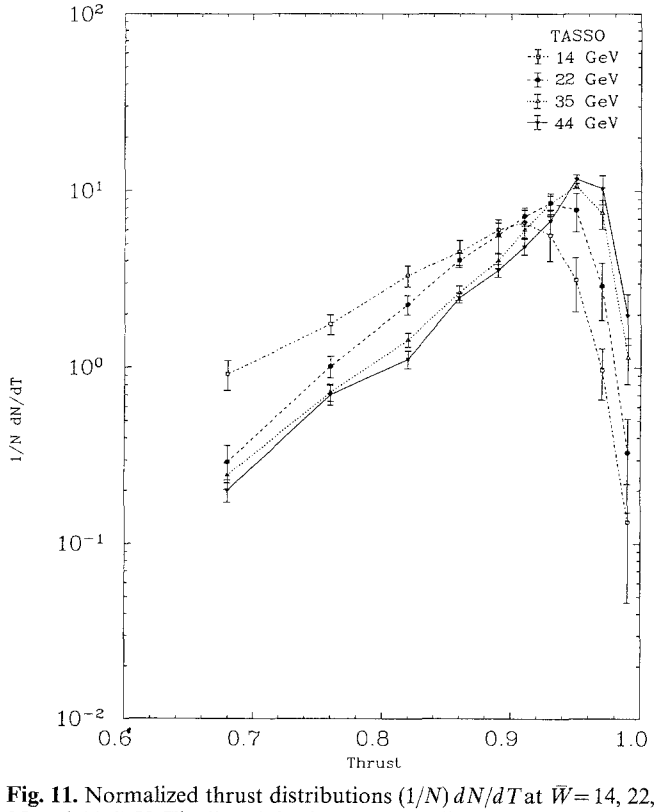

Fig. 11. Normalized thrust distributions $(1/N)\, dN/dT$ at $\bar{W}=14$, 22, 35 and 44 GeV. The lines join the corresponding points for clarity

Table 11. Normalized sphericity distributions $(1/N)\,dN/dS$

S	14 GeV	22 GeV	35 GeV	44 GeV
0.000–0.025	0.40 ±0.20	1.30 ±0.30	5.30 ±0.37	8.02 ±0.54
0.025–0.050	1.61 ±0.33	5.46 ±0.74	9.31 ±0.63	9.45 ±0.43
0.050–0.075	3.01 ±0.49	6.61 ±0.84	6.32 ±0.27	5.83 ±0.31
0.075–0.100	4.21 ±0.78	5.96 ±0.65	4.19 ±0.15	3.80 ±0.26
0.100–0.150	4.09 ±0.31	3.28 ±0.45	2.70 ±0.16	2.14 ±0.15
0.150–0.200	3.06 ±0.25	2.30 ±0.28	1.485 ±0.062	1.35 ±0.11
0.200–0.250	1.85 ±0.33	1.36 ±0.17	0.938 ±0.061	0.86 ±0.11
0.250–0.300	1.50 ±0.20	0.94 ±0.18	0.646 ±0.100	0.544 ±0.073
0.300–0.350	1.09 ±0.15	0.87 ±0.18	0.485 ±0.080	0.455 ±0.055
0.350–0.400	1.05 ±0.18	0.56 ±0.12	0.359 ±0.043	0.320 ±0.049
0.400–0.450	0.58 ±0.24	0.330 ±0.053	0.254 ±0.028	0.217 ±0.044
0.450–0.500	0.509 ±0.083		0.198 ±0.018	0.193 ±0.060
0.500–0.550	0.34 ±0.10	0.150 ±0.037	0.138 ±0.019	0.150 ±0.049
0.550–0.600	0.34 ±0.12		0.120 ±0.019	0.083 ±0.025
0.600–0.650	0.348 ±0.073	0.115 ±0.051	0.084 ±0.013	0.084 ±0.025
0.650–0.700			0.0469±0.0081	0.043 ±0.016
0.700–1.000	0.067 ±0.025	0.0104±0.0063	0.0082±0.0033	0.0079±0.0025
$\langle S \rangle$	0.2252±0.0075	0.1528±0.0075	0.1155±0.0047	0.1053±0.0035

Table 12. Normalized aplanarity distributions $(1/N)\,dN/dA$

A	14 GeV	22 GeV	35 GeV	44 GeV
0.00–0.01	5.8 ±1.5	11.2 ±1.9	25.4 ±1.7	35.3 ±1.9
0.01–0.02	12.8 ±2.9	20.6 ±2.4	28.4 ±2.6	28.4 ±2.1
0.02–0.03	14.0 ±1.7	18.0 ±1.7	17.00 ±0.65	14.9 ±1.1
0.03–0.04	12.8 ±1.2	15.5 ±1.5	10.30 ±0.65	8.3 ±1.1
0.04–0.06	9.97 ±0.98	8.9 ±1.2	5.25 ±0.88	3.59 ±0.87
0.06–0.10	4.43 ±0.71	3.05 ±0.38	1.43 ±0.32	1.08 ±0.33
0.10–0.15	2.16 ±0.37	0.78 ±0.16	0.37 ±0.11	0.180 ±0.060
0.15–0.20	0.68 ±0.14	0.210 ±0.065	0.083 ±0.025	0.046 ±0.025
0.20–0.30	0.32 ±0.16	0.039 ±0.023	0.0136±0.0053	0.0157±0.0080
$\langle A \rangle$	0.0613±0.0057	0.0386±0.0029	0.0261±0.0019	0.0213±0.0015

Table 13. Normalized thrust distributions $(1/N)\,dN/dT$

T	14 GeV	22 GeV	35 GeV	44 GeV
0.60–0.64	0.47 ±0.23	0.07 ±0.20	0.037 ±0.020	0.019 ±0.014
0.64–0.68	0.62 ±0.24	0.218 ±0.074	0.164 ±0.027	0.171 ±0.048
0.68–0.72	1.16 ±0.31	0.37 ±0.12	0.328 ±0.065	0.236 ±0.042
0.72–0.76	1.61 ±0.23	0.81 ±0.23	0.583 ±0.093	0.57 ±0.11
0.76–0.80	1.92 ±0.36	1.22 ±0.17	0.869 ±0.079	0.84 ±0.11
0.80–0.84	3.32 ±0.45	2.27 ±0.29	1.44 ±0.13	1.12 ±0.13
0.84–0.88	4.52 ±0.73	4.06 ±0.38	2.65 ±0.25	2.48 ±0.16
0.88–0.90	6.05 ±0.55	5.7 ±1.2	4.04 ±0.40	3.55 ±0.30
0.90–0.92	6.7 ±1.2	7.23 ±0.87	6.04 ±0.66	4.85 ±0.49
0.92–0.94	5.6 ±1.6	8.60 ±0.82	8.6 ±1.1	6.8 ±1.1
0.94–0.96	3.1 ±1.1	7.8 ±1.9	10.65 ±0.36	11.67 ±0.66
0.96–0.98	0.97 ±0.31	2.9 ±1.0	7.5 ±1.4	10.3 ±1.9
0.98–1.00	0.132 ±0.086	0.33 ±0.18	1.14 ±0.33	1.97 ±0.63
$\langle T \rangle$	0.8499±0.0085	0.8876±0.0073	0.9079±0.0045	0.9157±0.0049

the growth of the multiplicity with energy is due to the increase of low momentum particle production.

Figure 8 and Table 10 present the distributions of the transverse momentum with respect to the sphericity tensor axis. They become broader as energy increases.

5.4 Global event parameters

Figures 9–11 (Table 11–13) show the sphericity, aplanarity [10] and thrust [26, 27] distributions. All of them change with center of mass energy in a way which indi-

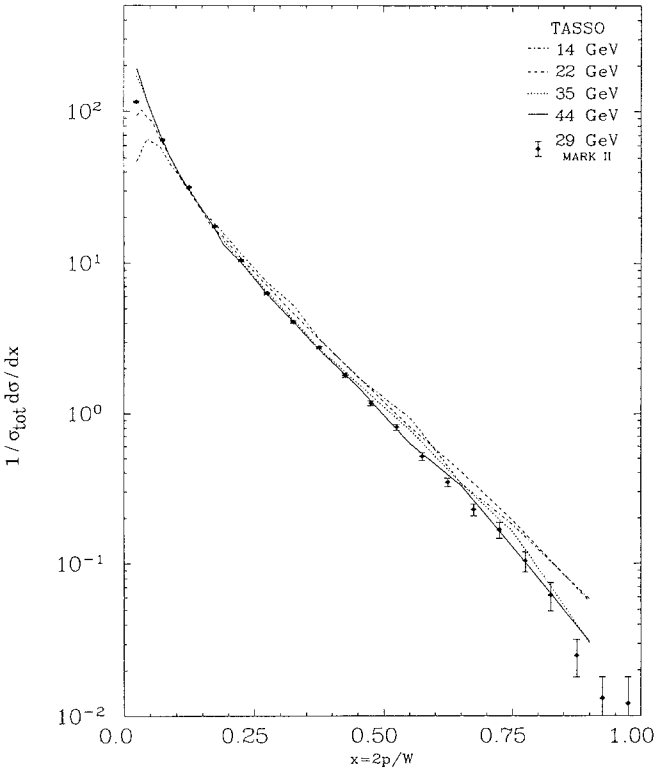

Fig. 12. Normalized scaled momentum distributions $(1/\sigma_{tot})\, d\sigma/dx$, where $x=2p/W$. TASSO (lines) and MARK II (points) data. The lines join the corresponding points, the error bars were removed for clarity

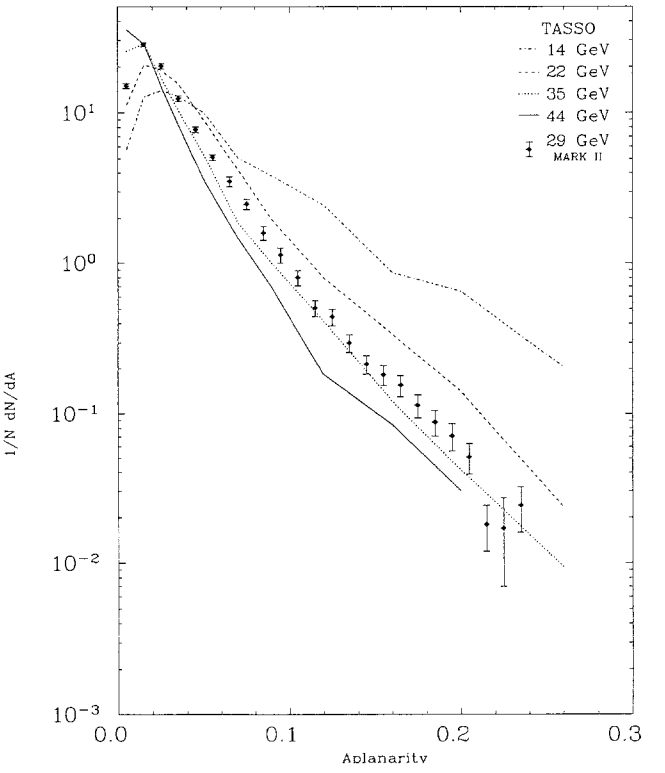

Fig. 14. Normalized aplanarity distributions $(1/N)\, dN/dA$. TASSO (lines) and MARK II (points) data. The lines join the corresponding points, the error bars were removed for clarity

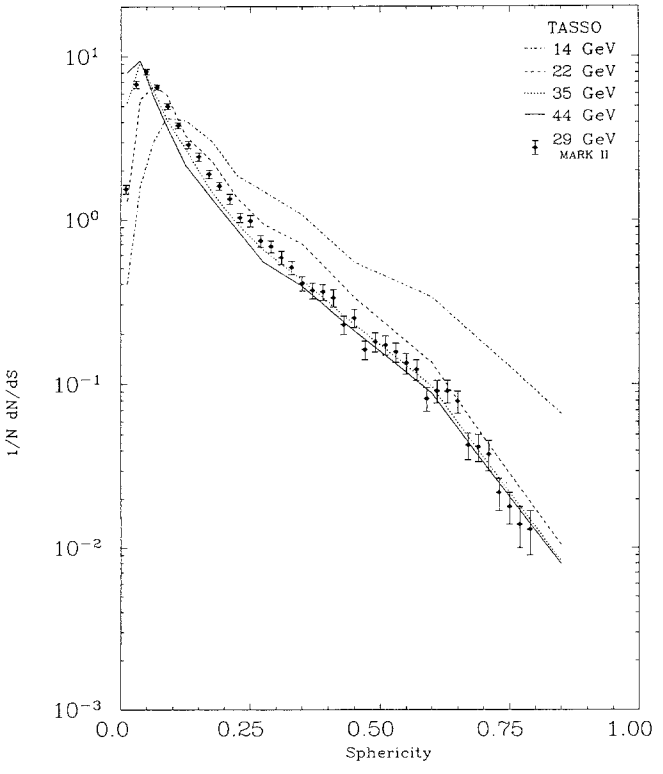

Fig. 13. Normalized sphericity distributions $(1/N)\, dN/dS$. TASSO (lines) and MARK II (points) data. The lines join the corresponding points, the error bars were removed for clarity

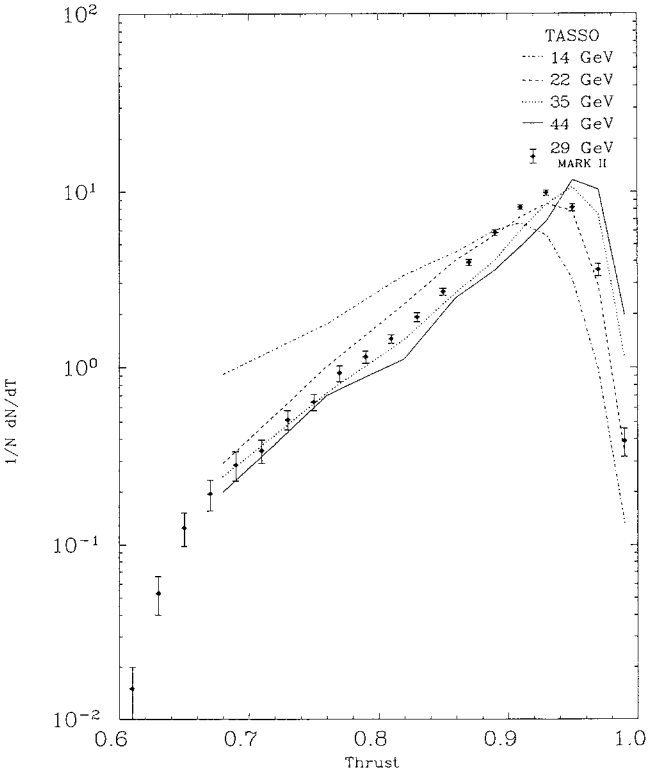

Fig. 15. Normalized thrust distributions $(1/N)\, dN/dT$. TASSO (lines) and MARK II (points) data. The lines join the corresponding points, the error bars were removed for clarity

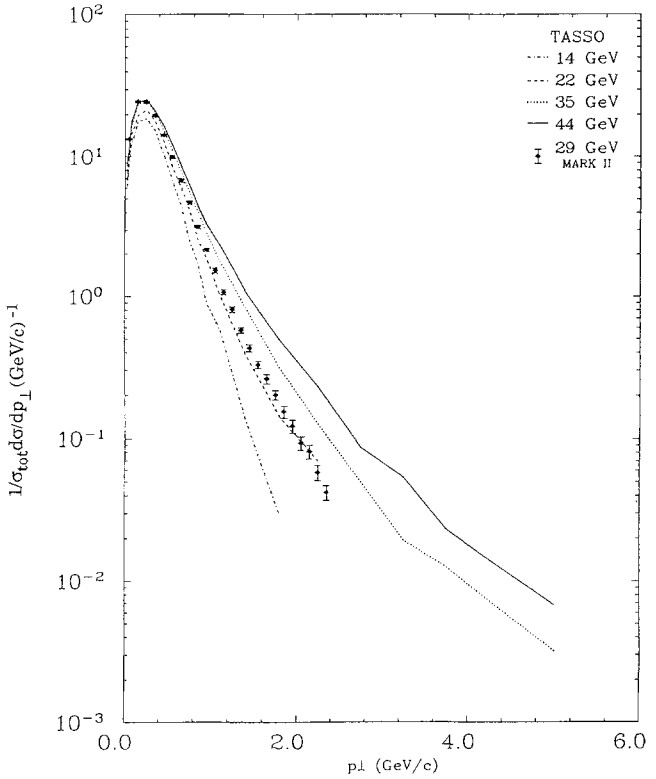

Fig. 16. Normalized transverse momentum distributions $(1/\sigma_{tot})\, d\sigma/dp_\perp$ (GeV/c)$^{-1}$. TASSO (lines) and MARK II (points) data. The lines join the corresponding points, the error bars were removed for clarity

cates that the events become more collimated with increasing energy.

The 14, 22 and 35 GeV results differ from the earlier [4] result. The difference comes mainly from the fact that the distributions are very sensitive to the Monte Carlo used to correct the data; in the past an independent jet $O(\alpha_s)$ Monte Carlo [28] was used, which does not reproduce the data so well. Since Lund LLA + $O(\alpha_s)$ Monte Carlo reproduces the data better, one can hope that the new distributions are closer to the true ones.

5.5 Comparison with MARK II

A comparison of the TASSO data with the MARK II [29] data is shown in Figs. 12–16, where the x, S, A, T and $p_\perp$ distributions are presented. The MARK II results for sphericity, aplanarity and thrust interpolate quite well between our data at 22 and 35 GeV; in the inclusive distributions the agreement is still reasonable.

6 Summary

In summary, jet properties at center of mass energies of 14, 22, 35 and 43.7 GeV were studied with the data collected in the TASSO detector. The total hadronic cross section ratio $\mathcal{R}$ at a center of mass energy of 43.7 GeV was found to be $\mathcal{R} = 4.11 \pm 0.05$ (stat.) ± 0.18 (syst.).

Corrected distributions of global shape variables such as sphericity, aplanarity, thrust and inclusive charged particle distributions of scaled momentum and transverse momentum were obtained. At all energies the same Monte Carlo event generator was used to calculate the corrections. At all energies the same correction technique was applied to avoid systematic biases.

Acknowledgements. We gratefully acknowledge the efforts of the PETRA machine group for high luminosity running, and the DESY directorate for their support. Those of us from abroad wish to thank the DESY directorate for the hospitality extended to us while working at DESY.

References

1. TASSO Coll. W. Braunschweig et al.: Z. Phys. C – Particles and Fields 41 (1988) 359
2. TASSO Coll. R. Brandelik et al.: Phys. Lett. 83 B (1979) 261
3. TASSO Coll. R. Brandelik et al.: Z. Phys. C – Particles and Fields 4 (1980) 87
4. TASSO Coll. M. Althoff et al.: Z. Phys. C – Particles and Fields 22 (1984) 307
5. T. Sjöstrand, M. Bengtsson: Comput. Phys. Commun. 39 (1986) 347
6. T. Sjöstrand, M. Bengtsson: Comput. Phys. Commun. 43 (1987) 367
7. M. Bengtsson, T. Sjöstrand: Phys. Lett. 185 B (1987) 435
8. F. Gutbrod et al.: Z. Phys. C – Particles and Fields 21 (1984) 235
9. TASSO Coll. M. Althoff et al.: Z. Phys. C – Particles and Fields 26 (1984) 157
10. J. Bjorken, S. Brodsky: Phys. Rev. D 1 (1970) 1416
11. G. Parisi: Phys. Lett. 74 B (1978) 65
12. B. Anderson et al.: Z. Phys. C – Particles and Fields 20 (1983) 317
13. C. Peterson et al.: Phys. Rev. D 27 (1983) 105
14. TASSO Coll. M. Althoff et al.: Phys. Lett. 146 B (1984) 443
15. TASSO Coll. M. Althoff et al.: Z. Phys. C – Particles and Fields 22 (1984) 219
16. F.A. Berends, R. Kleiss: Nucl. Phys. B 177 (1981) 231; B 178 (1981) 141
17. TASSO Coll. R. Brandelik et al.: Phys. Lett. 113 B (1982) 499
18. TASSO Coll. M. Althoff et al.: Phys. Lett. 138 B (1984) 441
19. CELLO Coll. H.-J. Behrend et al.: Phys. Lett. 183 B (1987) 400
20. JADE Coll. W. Bartel et al.: Phys. Lett. 160 B (1985) 337
21. MARK J Coll. B. Adeva et al.: Phys. Rev. D 34 (1986) 681
22. F.A. Berends et al.: Phys. Lett. 148 B (1984) 489
23. R. Baier, K. Fey et al.: Z. Phys. C – Particles and Fields 2 (1979) 339
24. G. Altarelli et al.: Nucl. Phys. B 160 (1979) 301
25. Yu.L. Dokshitzer et al.: Rev. Mod. Phys. 60 (1988) 373
26. S. Brandt et al.: Phys. Lett. 12 (1964) 57
27. E. Farhi: Phys. Rev. Lett. 39 (1977) 1587
28. P. Hoyer et al.: Nucl. Phys. B 161 (1979) 349
29. MARK II Coll. A. Petersen et al.: Phys. Rev. D 37 (1988) 1